Spatial Inhomogeneities in Emulsion Polymerizations: Repulsive Wall Calculations

Clive A. Croxton

Department of Mathematics, University of Newcastle, Newcastle, NSW 2308, Australia

Martin F. Mills,† Robert G. Gilbert,* and Donald H. Napper

School of Chemistry, Sydney University, Sydney, NSW 2006, Australia

Received December 4, 1992; Revised Manuscript Received February 26, 1993

ABSTRACT: The extent of the spatially inhomogeneous distribution of polymer particles in a latex formed by emulsion polymerization, dictated by thermodynamic considerations, is investigated computationally. Polymer chains suffer a loss of freedom near the particle surface, causing an entropic repulsion away from the surface and so favoring enhanced monomer concentration near the surface and thus polymerization by encapsulation. Thermodynamic calculations of the equilibrium polymer segment density distribution within a swollen latex particle show that while substantial entropic repulsions do occur, these are countered at higher polymer concentrations by polymer crowding effects. These calculations are performed using the iterative convolution technique to evaluate the segment–segment and segment–boundary correlations, corroborated where practicable with Monte Carlo calculations. This technique represents an advance over previous work which neglected polymer excluded-volume effects. Although the calculations were for low polymer fraction, trends from the results show that repulsive wall effects are highly unlikely to give rise to any significant inhomogeneities in latex particles formed from emulsion homopolymerization in conventional systems.

Introduction

In modeling the kinetics of emulsion polymerizations of a single monomer, one of the simplifying assumptions usually made is that the polymerization reaction occurs uniformly within the latex particles. The assumption of homogeneity is fundamental to most kinetic analyses and is employed in virtually all quantification and mechanistic interpretations of the emulsion polymerization process. If this assumption were proved to be generally invalid, most such studies would need to be reinvestigated. There are a number of circumstances where it is recognized that polymerization may be nonuniform: for example, where different monomer types are used in successive stages and incompatibility causes phase separation of the polymers. However, where only one monomer type is present which is fully miscible with its polymer, it is generally accepted that the system is homogeneous. Notwithstanding, as discussed in detail below, there have been a number of claims, based on both experiment and theory, that significant inhomogeneities exist in such particles. Much of this evidence is circumstantial and it has not been possible to answer definitively many of the questions which have arisen.

On the theoretical side, several mechanisms have been proposed to explain these results. One such is the "repulsive wall effect", which is thermodynamic in origin and forms the subject of the present paper; our thermodynamic modeling is through iterative convolution and Monte Carlo calculations of equilibrium polymer density distributions in swollen latex particles, including dependences on polymer chain length and concentration. Another effect, that of surface anchoring (which we here use to denote effects arising (a) because an entering free radical may have its end group, such as $-SO_4^-$, attached to the surface and (b) because of finite rates of diffusion of monomer and of polymer), is kinetic in origin and has been discussed by a number of workers,[1–3] including the present authors. A subsequent paper in our series will probe experimental aspects of the question using SANS.[4] In the repulsive wall effect, polymer chains that are located near the surface of a latex particle experience a loss of configurational degrees of freedom due to the confining effect of the surface. This causes an entropic repulsion of polymer chains away from the particle surface, leading to the monomer-swollen particle having a polymer-rich core surrounded by a monomer-rich shell. *In situ* polymerization of the resulting monomer distribution would be expected to give rise to particles having core–shell type morphology. The problem of modeling a concentrated polymer solution near a boundary is a complex one, and rigorous treatment has not been possible to date. However, a number of approximate theories have been used and these are now discussed.

Sperling and co-workers[5,6] performed random flight calculations for an isolated free-floating chain inside a spherical boundary, their results being found to support the existence of a strong entropic or repulsive wall effect pushing the polymer chains away from the particle surface and consistent with SANS data in the Guinier region. However, while this approach shows deviations from random flight conformations due to repulsive wall effects, it takes no account of excluded volume and other processes arising from polymer–polymer, polymer–solvent, and solvent–boundary interactions and would therefore seem to be of limited applicability in concentrated polymer solutions, such as are found in polymerizing latex particles. The question of sensitivity to inhomogeneity of these workers' SANS data has been discussed elsewhere.[4]

Scaling theory[7] has been used to formulate the expression:

$$\zeta_b = a\Phi_b^{(-0.75)} \tag{1}$$

for a semidilute system in contact with a repulsive wall. Here a is the lattice parameter, Φ_b is the volume fraction of the bulk polymer, and ζ_b is the correlation length of the bulk solution. Significant boundary effects were predicted only over distances approximately equal to the bulk correlation length. For a 5% by volume polymer solution,

* Author to whom correspondence is addressed.
† Present address: Technical Centre, Du Pont (Australia), Lot 15, Newton Rd., Wetherill Park, NSW 2164, Australia.

0024-9297/93/2226-3563$04.00/0

the correlation length is less than 5 nm. Since the above expression predicts that ζ_b decreases with increasing polymer concentration, the width of the depletion zone would be expected to become even smaller at polymer concentrations more representative of polymerizing emulsion systems.

Calculations for concentrated polymer solutions between parallel plates have been carried out using a mean-field analysis.[8] Effective single-chain statistics were formulated in terms of Gaussian partition functions. The treatment reduces to the Flory–Huggins form for ideal solutions in the unconfined limit, while in the dilute limit, the polymer concentration vanishes in the vicinity of the plates, as predicted by the classical diffusion (or random-walk) treatments.[9] Typically however, the polymer density profile is nonvanishing in the vicinity of the plates and tends to uniformity at higher polymer densities. Representative calculations were identified with polystyrene of molecular weight 20 000 with a plate separation of 16.8 nm and a polymer volume fraction of about 0.4. This is in the range of maximum repulsive wall effect according to the analysis of Yang.[10] The depletion layer at this concentration is less than 2 nm thick, dropping to a minimum concentration of about half the bulk. Although these calculations were solely for a planar boundary, this system is expected to show qualitatively similar behavior to a spherical boundary.

The theoretical evidence for significant inhomogeneities in typical latex particles is thus ambiguous. On the experimental side, Grancio and Williams[11] were the first to put forward evidence (as well as theoretical arguments) for the presence of significant repulsive wall effects. Staining techniques using a butadiene label were applied to study the morphology of two-stage styrene emulsion polymerizations. Results showed that most of the butadiene added was located near the surface after completion of the polymerization. Such morphology was observed over a wide range of particle sizes and (contrary to the results of Chen and Lee[12]) in systems where oil-soluble initiator was used, albeit to a lesser extent.[13] Further experiments were carried out in which tritium was used to label the seed, it being found that if the (nonlabeled) shell was sufficiently thick, emitted β-particles were unable to escape from the latex particle.[14]

If indeed repulsive wall effects cause extensive inhomogeneities in swollen latices, it follows that both the subsequent polymerization kinetics and final morphology may be affected. While the theoretical studies just cited give some idea of the effect of the particle boundary on the polymer, there is a need for more refined calculations. Random flight calculations do not give an adequate picture of these effects in concentrated polymer systems because they neglect polymer–polymer or excluded-volume effects. Conversely, while mean-field approaches are better suited to systems at higher polymer concentration, they assume ideality and neglect correlations between individual segments. Results are therefore of limited assistance in trying to gain a better mechanistic and predictive foundation. More involved approaches such as that of Myers et al.[15] are more difficult to apply to the systems in question.

The present study aims to investigate further the importance of repulsive wall effects by means of the iterative convolution (IC)[16] and Monte Carlo methods applied to simple model systems. The IC technique was developed to look at the statistical mechanics of short polymer chains and is readily extended to the present problem. Where practicable, Monte Carlo calculations are used in a complementary and confirmatory role. Perhaps more so than in most situations, the role of excluded-volume processes in determining the segment distribution in the vicinity of the particle boundary is central to any adequate calculation of intraparticle morphology. Here we explicitly incorporate these excluded-volume features. While the model systems used here are not truly representative of the system of interest (they are of necessity restricted to low molecular weights and low polymer volume fractions and may indeed overestimate the importance of excluded-volume effects), they overcome some of the problems inherent in the previous work and indicate trends applicable to the problem at hand. While results are limited to simple model systems, they represent an advance on the previous random flight calculations in that they include the effect of polymer excluded volume. These calculations help us to understand the role of these effects in determining monomer/polymer distributions within the latex particle and enable us to make predictions about their likely significance in real systems.

The Iterative Convolution Approach

Any adequate account of polymer segment density distribution within a particle should include the excluded-volume processes associated with the self-interaction of the polymer, the solvent–polymer interaction, and the interactions of polymer and solvent with the particle boundary. Here we investigate the effect of a spherical boundary on the configurational properties of a free-floating polymer sequence on the basis of the iterative convolution (IC) integral technique. In particular, we examine the effect of chain length (equivalent to molecular weight) and the number of chains upon the density profile and extend the discussion to include terminally attached sequences in which the self-avoiding chains are anchored to the rigid particle boundary.

We anticipate from the outset that regardless of the presence of a solvent or of excluded-volume processes, attrition of chain configurations as the sequences approach the particle boundary will establish an entropic repulsion on the chain, serving to deplete the segment density in the vicinity of the boundary wall. This entropic drive away from the boundary may be countered to a greater or lesser extent by a number of processes, particularly the excluded volume of the chains themselves.

The IC description is a correlation function approach based upon the iterative determination of the complete set of intersegmental spatial probability distributions $Z(ij|N)$ (where we adopt the notation $ij = r_{ij}$ throughout, without ambiguity), being the probability of finding particles i and j a distance r_{ij} apart for each pair of segments i,j within the N-mer. The only input required is the specification of the complete set of central, pairwise segment–segment interactions $\Phi(ij)$ (or their *effective* interactions $\Psi(ij)$ in the presence of a solvent; see below) within any heterogeneous (or, indeed, homogeneous) connected sequence of segments. The geometry of the macromolecule is established by specification of the sequential connectivity of the system. For a "necklace" of identical hard spheres, this is given by setting $Z(i,i+1|N) = \delta(r_{i,i+1} - \sigma)$ where $1 \leq i \leq N-1$ and σ is the segment diameter. The particular set of δ-functions specifies the geometry of the system: linear, ring, star, etc. The IC technique has been applied to numerous other problems,[17-20] and comparison of the IC description with the results of Monte Carlo simulation confirms that the technique appears to provide a good description of the configurational and scattering characteristics of self-interacting systems. Accordingly, we apply the IC technique to the present problem with confidence.

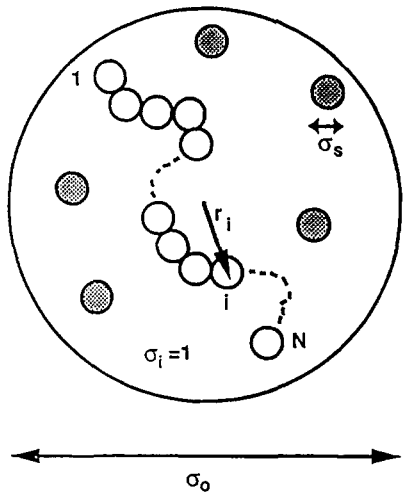

Figure 1. Schematic diagram of an occluded polymer chain.

We restrict ourselves to hard-sphere excluded-volume interactions in this analysis, although any central, pairwise interaction could in fact be used. The occluded linear chain is modeled as follows. The chain proper comprises 1, ..., i, ..., N identical hard-sphere segments of diameter $\sigma_i = 1$. Linear connectivity is established by setting $Z(i,i+1|N) = \delta(r_{i,i+1} - \sigma)$ where $1 \le i \le N$-1. These are occluded within a large spherical cell designated as "particle zero", of diameter σ_0 (see Figure 1). Thus we require that the location of the ith segment relative to the center of the cell is always such that $r_i \le (\sigma_0 - \sigma_i)/2$.

The IC equation itself is described elsewhere,[16,18-20] and so only a physical justification is given here. Consider two nonadjacent particles i and j in the chain. Neglecting for the moment all interactions in the system other than the direct interaction between these two particles, we may write to a first approximation:

$$Z(ij|N) \approx H_{ij} \equiv \exp(-\Phi(ij)/k_B T) \qquad (2)$$

where H_{ij} is the direct correlation between particles i and j and $\Phi(ij)$ is the pair potential, k_B is Boltzmann's constant, and T is the temperature. This expression is exactly true for two particles in a rarefied gas but must be modified in the presence of other particles. In a more concentrated system, $Z(ij|N)$ will be related to the potential of mean force, incorporating indirect effects due to the presence of other particles. In the IC approach, it is assumed that the total correlation function may be expressed as a product of H_{ij} with a correction for indirect effects via the remaining N-2 ($1 \ne i,j$) segments. For a given intermediate segment k, this correction is written as a convolution integral:

$$\int Z(ik|N)\, Z(kj|N)\, d\mathbf{r}_k \qquad (3)$$

The product $Z(ik|N)\, Z(kj|N)$ is in a sense a probability factor giving segment k's contribution to the indirect correlation between segments i and j. A product is used since this probability is *conditional* on the correlations of i with k AND k with j (i.e., the connectivity implies a relation between particles i and k AND particles k and j). By integrating over all possible positions of k, we are configurationally averaging the contribution of segment k (in probability terms, particle k can be at one $\mathbf{r}_k$ *or* another). In a simple fluid, the indirect correlation may be calculated via any representative third particle since they are all equivalent. In a polymer, however, each of the segments is unique by virtue of its differing position in the chain. This is an important point since it necessitates a knowledge of all of the $Z(ij|N)$'s in order to describe the system fully. This distinction also ensures differing contributions to the overall indirect effect, and accordingly we multiply H_{ij} by the geometric mean of N-2 convolution integrals in order to account for each of the indirect correlations between i and j via a third segment $k \ne i,j$.

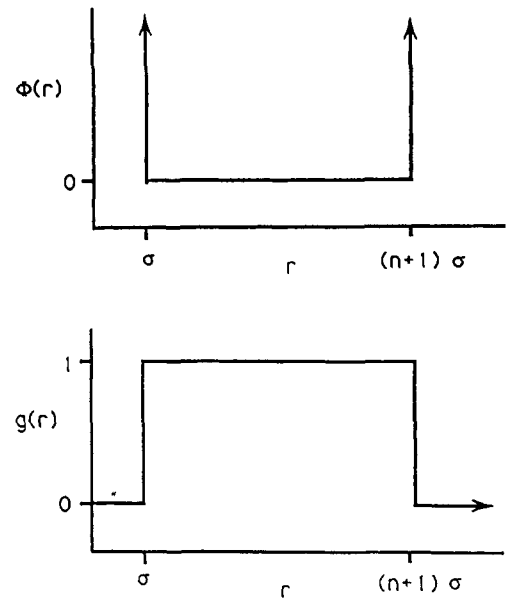

Figure 2. (Top) Potential between two hard-sphere segments i and j. (Bottom) Correlation between segments i and j for this potential.

$$Z(ij|N) = H_{ij} \prod_{k=0}^{N}{}' \int Z(ik|N)\, Z(kj|N)\, d\mathbf{r}_k \qquad (4)$$

Here, $\prod'$ represents the formation of the geometric mean for all k not equal to i,j and $\mathbf{r}_k$ is the position vector of the kth particle (i.e., it also involves a conditional "AND" probability). We must of course take into account all possible choices of a third particle; hence, the product $\prod'$ gives the compound effect of all indirect contributions (i.e., we require this condition for all particles k).

Solution of the IC Equation

Equation 4 is the central iterative convolution equation and may be solved exactly for a chain of three segments (see the Appendix). For more than three segments, the equations must be solved iteratively using fast Fourier transform techniques to evaluate the convolution integrals. This follows from the useful property of a convolution integral under Fourier transform—the convolution product reduces to a simple scalar product in reciprocal space. Thus by substituting the set of functions H_{ij} as a first approximation to $Z(ij|N)$ for each pair i,j and iterating to convergence, one obtains the complete set of spatial distributions and their associated moments such as the mean-square length, radius of gyration, scattering function, etc.

The H-functions for a hard-sphere potential may be represented simply by a Heaviside or step function having the value 0 for $r_{ij} < \sigma$ and 1 for $r_{ij} > \sigma$. Where segments i and j are connected via a sequence of other hard-sphere segments, we may replace this function with a top-hat form which is nonzero between σ and $n\sigma$ where n is the number of segments between i and j (Figure 2). This is made possible by the knowledge that, beyond this range, it would be necessary to break the chain in order to move segments i and j any further apart; this H thus already explicitly incorporates some of the indirect contributions to the potential (see the Appendix).

While the approximate treatment of eq 4 appears to work well for short chains, there are limitations on the length of chains which may be studied by this technique. This is a consequence of reducing the many-body problem to a function of two-body interactions. The longer the chain, the more indirect interactions there are to take into account and so the more inadequate the approximation becomes. The possibility of improving the approximation to enable extension to longer chains is currently being investigated.

In the presence of a solvent, the segment–segment and segment–boundary interactions become progressively modified with increasing solvent packing fraction, $\Phi(ij)$ then being replaced by an *effective* interaction $\Psi(ij)$, the potential of mean force. Such a modification is familiar in the theory of single-component simple fluids where the radial distribution function is related via the Boltzmann equation to the potential of mean force: $g_{(2)}(ij) = \exp(-\Psi(ij)/k_BT)$, which is also characterized by $\Phi(ij) \rightarrow \Psi(ij)$ with increasing the packing fraction. In the present problem we recognize that we are dealing with a three-component system comprised of a hard-sphere occluding particle of diameter σ_0, chain segments (monomers) of diameter σ_i at packing fraction η_i immersed in a solvent of hard spheres of diameter σ_s at packing fraction η_s. Now, the *fluid* radial distribution $g^{\alpha\beta}_{(2)}(ij)$ between any two particles of species α,β (and hence the associated potential of mean force $\Psi(ij)$) within an r-component system is given by the coupled set of Ornstein–Zernike equations[21]

$$h_{\alpha\beta}(1,2) = c_{\alpha\beta}(1,2) + \sum_{\gamma=\alpha}^{\rho} \rho_\gamma \int h_{\beta\gamma}(23)\, c_{\alpha\gamma}(13)\, d\mathbf{r}_3 \quad (5)$$

where c is the direct correlation function defined in the Percus–Yevick approximation as

$$c^{PY}_{\alpha\beta}(ij) = g^{\alpha\beta}_{(2)}(ij)\left(1 - \exp\left(-\frac{\Phi_{\alpha\beta}(ij)}{k_BT}\right)\right) \quad (6)$$

and the number density ρ_i of a species is related to its packing fraction η_i by $\eta_i = \pi\rho_i\sigma^3/6$, $c_{\alpha\beta}(ij)$ is the direct correlation between two particles of species α,β at separation r_{ij}, and $h_{\alpha\beta}$ is the total correlation: $g^{\alpha\beta}_{(2)}(ij) = h_{\alpha\beta}(ij) + 1 = H_{\alpha\beta}(ij)$. By elementary matrix manipulation of the coupled set of equations (eq 5), the principal effective H-functions (incorporating the modification caused by the solvent) may be determined on the basis of a Percus–Yevick approximation for $c_{\alpha\beta}(ij)$ (eq 6) to yield (for our problem) the solvent–polymer, solvent–boundary, and polymer–boundary potentials of mean force. (Here, solvent, polymer, and the boundary itself are each treated as separate components.) These effective H-functions which incorporate solvent effects are then substituted into the IC equation to obtain the Z-functions for polymer chains immersed in a solvent.

The PY approximation is known to be particularly good for the description of hard-sphere interactions.[21] Thus, in evaluating the IC equations, the segment–segment and segment–boundary interactions develop via the appropriate potentials of mean force which reflect the multicomponent screening which develops in high-density fluid mixtures. It should be emphasized that this approach models the potentials of mean force as if the constituent particles were part of a multicomponent *fluid*. It is difficult to assess the effect of segmental connectivity of one component of the system upon the final estimate of the effective interaction. Nevertheless, this approach should yield a good first-order estimate of the multicomponent aspects of the system. It is appropriate to point out that the problem is considerably simplified by the fact that the solvent packing fraction η_s is much greater than η_0 and η_i (the boundary and segment packing fractions, respectively), and so we may set $\eta_0 = \eta_i = 0$ in the solution of eq 5. Note that this does *not* prohibit the determination of distributions with respect to species 0, i.

We now solve the set of IC equations (eq 4) by using the H-functions determined on the basis of the Ornstein–Zernike equations (eq 5) in the Percus–Yevick approximation (eq 6) and determine the various distributions and their moments as a function of the solvent diameter and packing fraction. The segment density distributions are calculated as a function of chain length (molecular weight) and multiplicity (number of chains). Multiplicity, in the case of a system of n identical chains, is handled by allowing the index k in eq 4 to range through *two* chains, thereby accounting for all intra- and interchain correlations. The second chain is seen as a representative sequence, and contributions arising from second and subsequent sequences to the convolution product in eq 4 are accorded the power n in forming Π'. This asserts the chains all behave identically. If the chains are distinct for whatever reason, then the appropriate number of *kinds* of interaction must be explicitly incorporated in forming the convolution product.

Monte Carlo Calculations

Where possible, Monte Carlo calculations have been used in support of IC results and it is noted here that consistent agreement has been obtained previously between MC and IC calculations for a variety of systems. The Monte Carlo result is in effect an exact solution of the problem, providing a sufficient number of configurations is obtained to minimize statistical errors, and may in principle be extended to any chain length or number of chains. In practice (as will be seen shortly), a progressively larger proportion of configurations will be rejected with increasing numbers of segments and so calculations are severely restricted by the amount of computational time required.

The procedure used to generate one configuration for a single free-floating chain is as follows:

(1) Randomly select the position of the first segment within the particle boundary.

(2) Randomly select the position of the second segment subject to the additional restriction that the distance between the two segments is fixed (i.e., the segments are attached to one another).

(3) Continue adding segments as in step 2, checking for each segment that no overlap occurs with other segments or the particle boundary until the chain (or configuration) is complete.

If, at any stage, an overlap does occur, the entire configuration must be rejected and recommenced at step 1. Since only those configurations which are successfully completed with no overlap occurring are accepted, segments located further along the chain have no "knowledge" of previous segments and so selection of the configuration in this manner is truly random.

For a random walk, the radius of interaction is zero and so segment overlap is "allowed", while for hard-sphere calculations, the radius is taken to be half the segment length. Accordingly, the hard-sphere and random-walk models can be considered to represent respectively upper and lower limits for the level of excluded volume likely to be present in real systems.

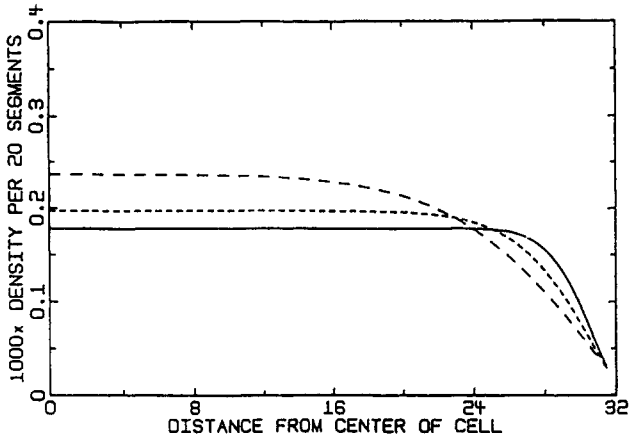

Figure 3. IC segment density profile for a single hard-sphere sequence in a particle of radius 32 segments. (—) 5 segments in chain. (· · ·) 10 segments in chain. (- - -) 20 segments in chain.

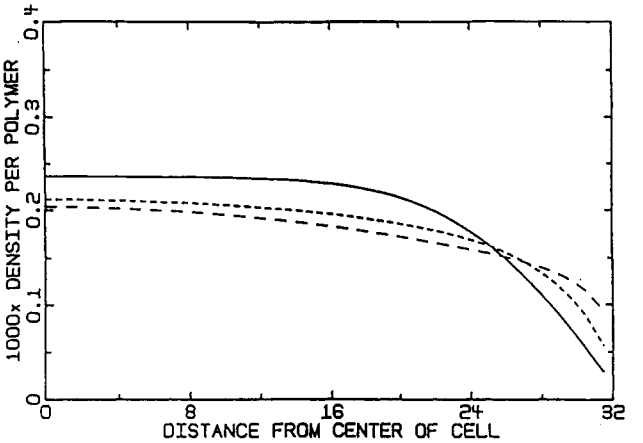

Figure 4. IC segment density profile for M chains for 20 segments in a particle of radius 32 segments. (—) $M = 1$. (· · ·) $M = 5$. (- - -) $M = 20$.

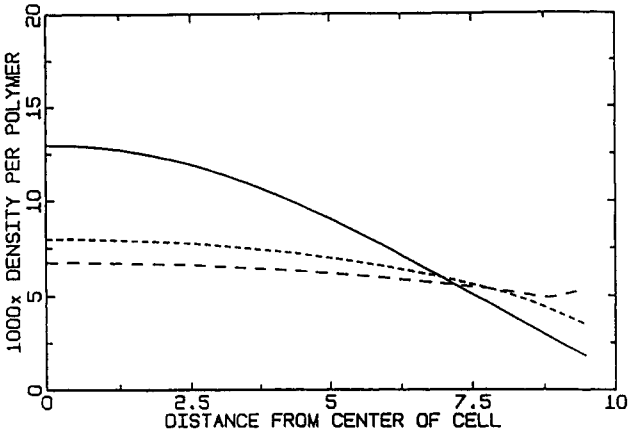

Figure 5. IC segment density profile for M chains of 20 segments in a particle of radius 10 segments. (—) $M = 1$. (· · ·) $M = 5$. (- - -) $M = 20$.

Multiple chain configurations may be obtained in a fashion similar to that above by generating each chain in succession with rejection of the entire configuration if at any point in generating the configuration any intra- or interchain interaction occurs. Needless to say, this process tends to be very inefficient and computational time rises very sharply with the number of segments in the chain. Efficiency may be increased considerably if it is recognized that intrachain interactions of the type i,i-2 are geometrically predetermined and hence independent of the chain configuration. Therefore, if an i,i-2 overlap occurs when generating a configuration, it is permissible to make another selection of the position of the ith particle (if no other violations have occurred) rather than reject the entire configuration. The probability of an i,i-2 overlap is of course fixed, having a value of 0.125. Therefore, the probability of generating a chain without at least one such overlap occurring in a chain of length N is $(0.9)^N$, which for a chain of length 100 would mean only $\sim$1 in 10^6 configurations would be allowable on the basis of this interaction alone.

Results: Iterative Convolution Calculations

The segment density profile relative to the center of the large particle (designated particle "0") is used to quantify the extent of attritional effects and, for the IC calculation, is given by

$$\rho(r|N) = \sum_{i=1}^{N} Z(0i|N) \tag{7}$$

where the $Z(0i|N)$ are the normalized spatial distributions of the i segment particles sequentially connected to form an N-mer within the large occluding particle.

Figure 3 shows the segment density profiles for single self-avoiding hard-sphere sequnces of 5, 10, and 20 monomers occluded within a large particle in the absence of solvent. Density depletion near the boundary due to chain attrition is clearly apparent, and its spatial extent is seen to increase with the size of the chain or R_g, the radius of gyration. In this regard, the IC calculations are found to be in qualitative agreement with random flight results.[10] As the number M of chains increases (M = 5 and 20 in Figure 4), still in the absence of a solvent, we find the density depletion at the boundary decreases in both range and magnitude. The segment density profile becomes more uniform throughout the occluding particle, and this we attribute to the excluded-volume effects operating throughout the interior of the particle, countering the attritional effects at the boundary. In the random flight representation, only surface attritional effects arise, since the chains are otherwise totally noninteracting and geometrical crowding effects do not occur.

In relating the present calculations to a representative latex system in which the polymer volume fraction is typically in the range 30–100%, it is noted that the 20-chain result in Figure 4 corresponds to a total polymer volume fraction of $\sim$0.15%. The number and/or length of chains could not be substantially increased in the present calculations due to the known limitations of the IC approximation. However, the effective volume fraction may be increased by reducing the diameter of the confining particle.

For a cell of diameter 40 segments, similar qualitative trends with chain number as for the 64 unit cell are observed. The 20-chain result shows reduction in the concentration gradient in the vicinity of the boundary when compared to the larger cell, and this trend is continued on going to an even smaller cell. Figure 5 shows the result for a cell of diameter 20 segments, corresponding to a volume fraction of polymer of $\sim$5%. We observe that the competing effects of volume exclusion within the interior and attritional effects at the boundary of the particle result in a progressive decrease in the extent of polymer depletion with increasing polymer fraction. The role of excluded volume in this process is crucial, and the result could not have been anticipated on the basis of random flight calculations. If the trends observed here were continued to polymer fractions of 30% and higher, it might reasonably

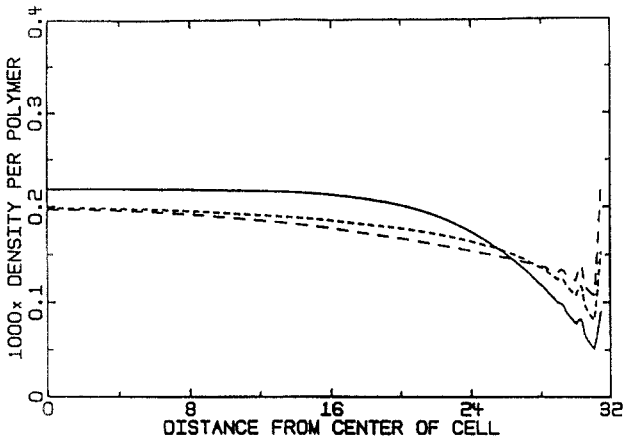

Figure 6. IC segment density profile for M chains of 20 segments in a particle of radius 32 segments with a solvent at packing fraction 0.4. (—) $M = 1$. (···) $M = 5$. (- - -) $M = 20$.

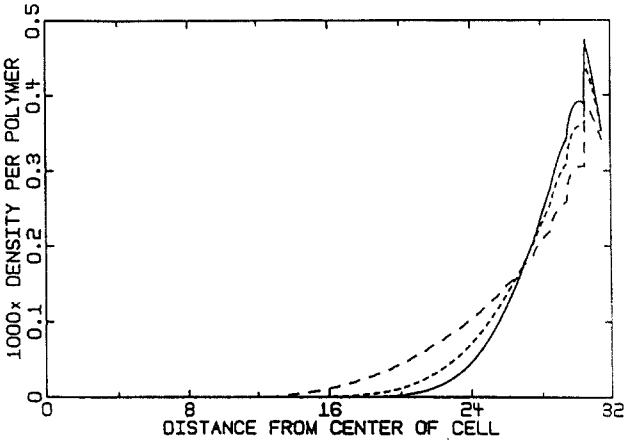

Figure 7. IC segment density profile for M terminally attached chains of 20 segments in a particle of radius 32 segments. (—) $M = 1$. (···) $M = 5$. (- - -) $M = 20$.

be expected that the concentration gradients would become negligible and therefore unimportant with regard to the kinetics of polymerization and the morphology. The restriction of the chain length to 20 segments does not appear to pose any difficulty here as the conclusions should be qualitatively the same regardless of chain length.

With the introduction of hard-sphere solvent particles, particularly at high packing fractions η_s, solvent layering effects at the boundary are of course inevitable. These structural features impose a corresponding structural response upon the polymer segment density distribution with an oscillatory structure, of the same period as the solvent layering, developing within $\sim 3\sigma_s$ of the particle boundary (Figure 6). These structural features are entirely consistent with earlier calculations for terminally attached chains at a rigid boundary.[22] Nevertheless, the mean segment density profile shows the same qualitative behavior as described above in the absence of a solvent. It should be observed that more realistic softer interactions between solvent, segments, and the particle boundary would result in a substantial relaxation of the structural features reported here which arise from the hard-sphere representation of the repulsive component of the interaction. The hard-sphere potential clearly also overestimates the excluded volume. Nevertheless, these calculations clearly indicate the role of excluded-volume processes operating throughout the system which is entirely neglected in the random flight representation.

One possibility which should be addressed is that polymer chains may be terminally attached to the particle surface: the surface anchoring effect.[1-3] This situation may arise in latex systems because polymer chains originating from aqueous-phase initiator (such as persulfate) will have an end group which is charged and therefore hydrophilic. Inspection of IC calculations for terminally attached chains of length 20 segments (Figure 7) shows that the polymer segment density actually increases toward the particle surface (which is the opposite trend to that observed for free-floating chains). It appears however that this conclusion is slightly misleading, and, as will be seen later, there may also be depletion at the boundary for attached chains. Regardless of the shape of the profile, trends toward uniformity similar to those seen for unattached chains are seen with increasing the polymer fraction. The true situation in an emulsion polymerization is likely to be somewhere between the free-floating and terminally attached cases presented here. Polymer chains produced by growth of monomeric free radicals created by transfer may be free floating while those having terminal sulfate groups will tend to be anchored at the surface. Some may even be attached at both ends of the chain. This will depend on the relative rates of transfer and termination in the system and on the fate of short free radicals produced by transfer.

Results: Monte Carlo Calculations

Monte Carlo calculations were carried out for single random flight and hard-sphere chains of up to 80 segments in length. Results are given in Table I and Figure 8, it being found that, for hard-sphere calculations, reasonable qualitative agreement with IC results is obtained (although the IC calculations tend to overestimate slightly the width of the depletion layer).

As the molecular weight is increased, the depletion width continues to grow with the R_g as expected. It is also noted that for random flight calculations, the theoretically predicted value of R_g ($=\sigma(N/6)^{1/2}$) is obtained (where σ is the length per segment and N is the number of segments in the chain) except for very small particles where the level of confinement causes some contraction of the polymer coil.

MC calculations for multiple chains were limited in scale because of the computational time required (up to 7 days of cpu on an Apollo 10000). Nevertheless, some results were obtained for very short chains, showing qualitatively the same tendency toward uniform distribution with increasing the packing fraction as was observed for the IC calculations (Figure 9). It is noted that results are somewhat noisy because of the limited number of configurations obtained. The noise tends to be most pronounced near the center of the particle where fewer segments are included in the averages because of the reduced volume available at smaller radii. Fortunately this is not the region of greatest interest in the present calculations. The volume fraction of polymer in this calculation is about 1% for the three-chain result, and it was found that, for the MC calculations, this was the minimum concentration necessary for crowding to have an observable effect on the distribution. In fact, this appears to be the point at which the chains start to overlap. It appears therefore that the IC calculations may overestimate slightly the extent of crowding which occurs at low polymer concentrations. These discrepancies seem to be related to the observed errors in depletion width for a single chain and probably arise from the averaging procedure used to account for interactions with the second chain (interactions which should only apply when the chains are in actual contact). Note that the onset of crowding may vary with chain length.

Table I. Calculated Depletion Widths and Radii of Gyration[a]

method	segment type	N	particle radius	R_g	D_{50}	R_g(theo)[b]
IC	hard sphere	5	32	0.98	1.6	0.91
IC	hard sphere	10	32	1.55		1.29
IC	hard sphere	20	32	2.64	4.5	1.83
MC	hard sphere	10	32	1.69		1.29
MC	hard sphere	20	32	2.69	2.3	1.83
MC	hard sphere	50	32	4.84	4.0	2.89
MC	hard sphere	80	32	6.45	5.6	3.65
MC	random walk	80	32	3.62	3.3	3.65
MC	random walk	20	32	1.81	1.4	1.83

[a] D_{50} is the point at which the polymer concentration is halfway between that in the bulk and that at the surface. [b] R_g(theo) is the predicted R_g for a random coil.

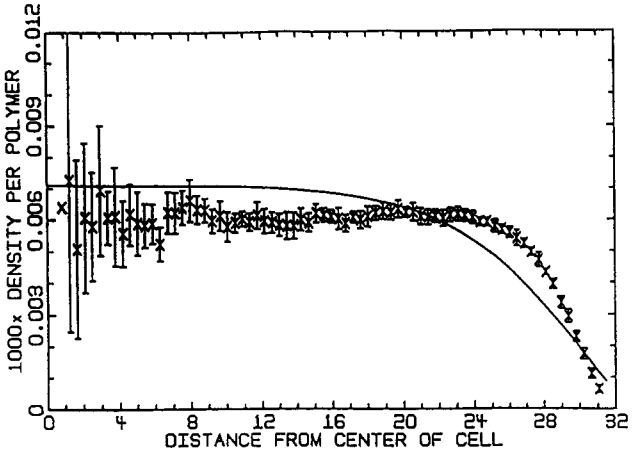

Figure 8. Comparison of iterative convolution and Monte Carlo results for a chain of 20 segments in a cell of radius 16. (—) IC. (×) MC.

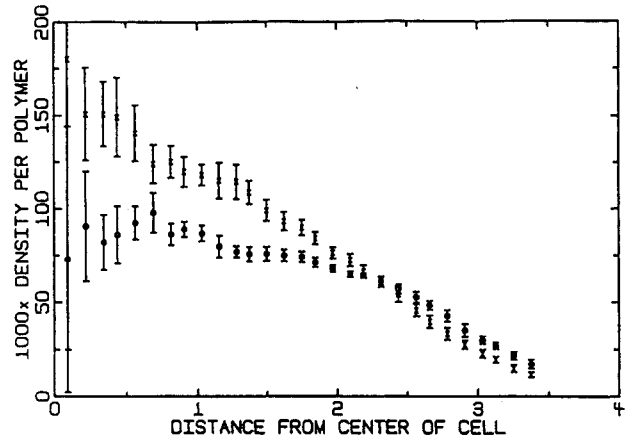

Figure 9. Monte Carlo segment density profile for M chains of 8 segments in a particle of radius 4 segments. (×) M = 1. (○) M = 3.

Results for attached chains (Figure 10) show that, as the chain becomes longer, a maximum in the density distribution is observed at a distance from the surface which is again related to the length of the chain and increases with the R_g. This however does not alter the fact that, as the volume fraction of polymer is increased, the distribution will again tend to uniformity because of increasing polymer–polymer interactions.

Conclusions

Calculations of the intraparticle polymer segment density distribution for single hard-sphere free-floating chains (including all interactions between polymer, solvent, and boundary) show significant polymer depletion near the particle surface due to attritional effects in the vicinity of the repulsive wall. The spatial extent of the depletion

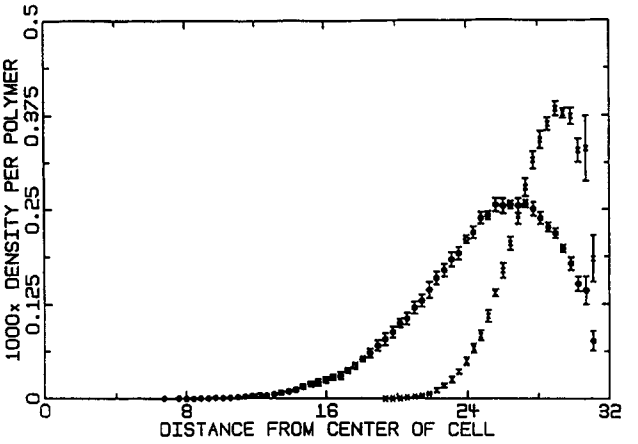

Figure 10. Monte Carlo segment density profile for a terminally attached chain in a cell of radius 32. (×) 20 segments in chain. (○) 50 segments in chain.

region is seen to be related to the chain length or size of the polymer coil. To this extent, the random flight and excluded-volume calculations are in qualitative agreement. However, on increasing the polymer volume fraction, attritional effects are progressively countered by geometric packing effects throughout the volume of the particle, whereupon the segment density profile becomes more uniform, to the point where very little solvent concentration gradient would be expected at polymer concentrations such as are found in polymerizing latex particles.

Although the results presented here are limited to very short chains and low polymer concentrations, it is expected that the basic *principles* described herein are applicable to any molecular weight or polymer volume fraction. These calculations show that, with increasing polymer fractions and molecular weights, repulsive wall effects become negligible; these trends therefore are strongly indicative that the same conclusion will hold for "real" systems with much higher polymer fraction and molecular weights than those employed in the present computations. While the width of the depletion region increases with molecular weight, both the width and depth are observed to decrease with increasing polymer concentration. It is not possible to predict precisely how large the depletion layer will be at the much higher polymer concentrations found in latex particles, but it seems unlikely that it will be significant (even when taking into account the probable overestimation of excluded volume in the present calculations).

The present calculations predict negligible depletion due to repulsive wall effects at higher molecular weights; however, they are restricted by being for relatively small numbers of low molecular weight chains at low polymer concentrations. Nevertheless, the *trends* enable definite conclusions to be drawn for real systems. Figures 3 and 10 show that the depletion layer is reduced with increasing

the molecular weight (all other factors being constant); Figures 4–7 show that depletion is reduced with increased number of chains (all other factors being constant); and Figures 4–7 and 9 show that depletion is reduced with increasing the polymer concentration (all other factors being constant). Hence we can *rigorously* state that there are highly likely to be negligible inhomogeneities in latex particles made from a single monomer under virtually all conditions expected to be encountered in practical systems. This is in contradistinction to the predictions of random flight calculations;[5,6] however, the neglect of excluded volume in random flight calculations restricts the description to the attritional effect of the depletion zone. Clearly all polymer–solvent–boundary effects should be included in calculations if the random flight model is to be realistic at higher polymer concentrations.

Mean-field and scaling theories which are used to predict average properties for systems in this concentration regime apply terms such as correlation and screening length to quantify the length scales of polymer–polymer and polymer–boundary interactions. It would seem that, at higher polymer concentrations, close-range intra- and interpolymer excluded-volume interactions become increasingly dominant in determining polymer conformations. It is because of the dominance of such short-range interactions at high polymer concentrations that these "average" descriptions might be expected to give a fair representation of the actual density distribution. The present study, however, makes no such averaging assumptions and looks at the correlations between each of the individual segments. The IC techniques therefore offer more opportunity for mechanistic understanding than these approximate treatments.

The roles of repulsive wall and excluded-volume effects are of considerable importance in understanding both the polymerization kinetics and the final morphology of the latex in emulsion homopolymerizations. If, as random flight calculations suggest, there were significant intraparticle concentration gradients present, the rates of diffusion, propagation, and termination would be dependent on the position within the latex particles. This would have far-reaching implications with regard to currently accepted kinetic models and parameters since it would no longer be valid to assume homogeneity except in special cases. Fortunately, the present calculations show that this is not likely to be a problem and conventional kinetic treatments should be accurate. Moreover, such conclusions are consistent with the results of SANS experiments.[4]

Acknowledgment. The financial support of the Australian Research Grants Committee and of an Australian Postgraduate Research Award for M.F.M. is gratefully acknowledged. We greatly appreciate the assistance of Ruby Turner in the computations and stimulating discussion with Dr. Jeff Reimers.

Appendix: Solution of the Iterative Convolution Equation for a Three-Segment Chain

While the iterative convolution equation (eq 4) does not in general admit of an analytic solution, it is possible to solve the equations analytically for the special case of a single free-floating chain of 3 segments. This is of interest since it gives some insight into the workings of the equation and establishes its validity at least in this limiting case. For this system, the equations reduce to the following:

$$Z_{13} = H_{13}\int Z_{12}Z_{23}\,d\mathbf{r}_2 \qquad \text{(A1)}$$

Now since correlations between neighboring segments are defined as a δ-function, we may say $Z_{12} = H_{12} = \delta(r_{12} - \sigma)$, and likewise for Z_{23}. Referring now to Figure 11, it can be seen that segment 2 is constrained to move on a circle of radius $L = (\sigma^2 - (r_{13}/2)^2)^{1/2}$ orthogonal to the vector $\mathbf{r}_{13}$ and centered at its midpoint. Since we may define our axis system in any way we please, we now select it in such a way that this circle lies in the $z = 0$ plane. The convolution integral may now be rewritten:

$$\int Z_{12}Z_{23}\,d\mathbf{r}_2 = \int dx_2\,dy_2\,dz_2\,\delta(z_2{=}0) \times \delta(x_2^2{+}y_2^2{-}[\sigma^2{-}(r_{13}/2)^2]) \qquad \text{(A2)}$$

Converting to polar coordinates, this becomes

$$\int Z_{12}Z_{23}\,d\mathbf{r}_2 = \int_0^\infty r_2\,dr_2 \int_0^{2\pi} d\theta_2\,\delta(r_2^2{-}[\sigma^2{-}(r_{13}/2)^2]) = 2\pi[\sigma^2 - (r_{13}/2)^2]^{1/2} \qquad \text{(A3)}$$

This function is plotted together with H_{13} in Figure 12, where it can be seen that the function is increasing as particles 1 and 3 approach to within the hard-sphere distance σ. Note that the function is not defined outside $r_{13} = 2\sigma$. This is to be expected as the connectivity of the chain would otherwise be destroyed. The product of H_{13} (note no inference about the connection of segments 1 and 3 via segment 2 has been included in this function) with the convolution integral gives our desired function Z_{13}. The form of Z_{13} shows an increase as segments 1 and 3 approach because of entropic considerations—the number of possible configurations at a given distance r_{13} decreases with increasing r_{13} since segment 3 can only move on a circle of diminishing diameter. In the limiting case where $r_{13} = 2\sigma$, segment 3 can only occupy one point in space. Z_{13} therefore incorporates the potential of mean force between segments 1 and 3 including the indirect effect of segment 2. If the above equations are solved in only two dimensions, a simpler top-hat form of Z_{13} is

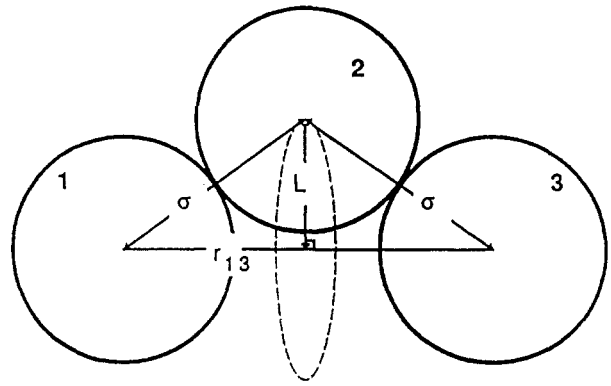

Figure 11. Representation of a 3-segment chain.

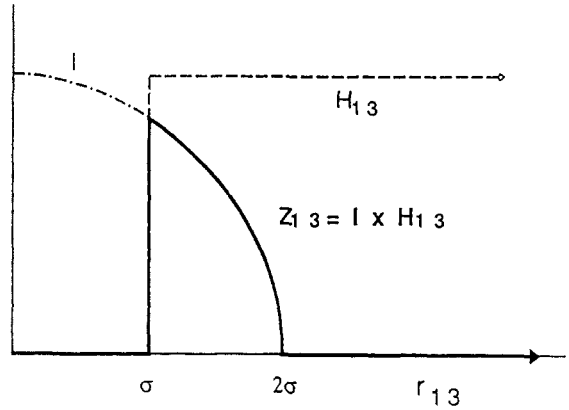

Figure 12. Correlation function Z_{13} for a 3-segment chain. I is the convolution integral.

obtained because of the reduced degrees of freedom. Truncation of H_{ij} at $(i-j)\sigma$ is justified for the special case of hard-sphere segments, since physically the segments cannot be any further apart, and this is borne out by the above derivation. The same result should be obtained whether top-hat or Heaviside functions are used for H_{ij} as the convolution integrals should ensure the correct range for Z.

References and Notes

(1) Chern, C. S.; Poehlein, G. W. *J. Polym. Sci., Polym. Chem. Ed.* **1987**, *25*, 617.
(2) Mills, M. F.; Gilbert, R. G.; Napper, D. H. *Macromolecules* **1990**, *23*, 4247.
(3) de la Cal, J. C.; Urzay, R.; Zamora, A.; Forcada, J.; Asua, J. M. *J. Polym. Sci., Polym. Chem. Ed.* **1990**, *28*, 1011.
(4) Mills, M. F.; Gilbert, R. G.; Napper, D. H.; Rennie, A. R.; Ottewill, R. H. SANS studies of morphology, submitted for publication in *Macromolecules*.
(5) Dabdub, D.; Klein, A.; Sperling, L. H. *J. Polym. Sci., Part B: Polym. Phys.* **1992**, *30*, 787.
(6) Yang, S. I.; Klein, A.; Sperling, L. H. *J. Polym. Sci., Polym. Phys. Ed.* **1989**, *27*, 1649.
(7) de Gennes, P.-G. *Macromolecules* **1981**, *14*, 1637.
(8) Ronca, G. *J. Appl. Polym. Sci.* **1987**, *33*, 2623.
(9) Di Marzio, E. A. *J. Chem. Phys.* **1965**, *42*, 2101.
(10) Yang, S. I.; Klein, A.; Sperling, L. H.; Casassa, E. F. *Macromolecules* **1990**, *23*, 4582.
(11) Grancio, M. R.; Williams, D. J. *J. Polym. Sci., Part A-1* **1970**, *8*, 2617.
(12) Chen, S. A.; Lee, S. T. *Makromol. Chem., Rapid Commun.* **1990**, *11*, 443.
(13) Keusch, P.; Williams, D. J. *J. Polym. Sci., Polym. Chem. Ed.* **1973**, *11*, 143.
(14) Keusch, P.; Graff, R. A.; Williams, D. J. *Macromolecules* **1978**, *7*, 304.
(15) Myers, K.; Nemriovsky, A. M.; Freed, K. F. *J. Chem. Phys.* **1991**, *95*, 6112.
(16) Croxton, C. A. *J. Phys. A: Math. Gen.* **1984**, *17*, 2129.
(17) Fleming, R. J., submitted for publication in *J. Phys. A.: Math. Phys.*
(18) Croxton, C. A. *Macromolecules* **1988**, *21*, 3023.
(19) Croxton, C. A. *Macromolecules* **1988**, *21*, 244.
(20) Croxton, C. A. *Macromolecules* **1988**, *21*, 2269.
(21) McQuarrie, D. A. *Statistical Thermodynamics*; Harper and Row: New York, 1983.
(22) Croxton, C. A. *Macromolecules* **1987**, *20*, 2847.